Stretchable, Transparent, Ultrasensitive, and Patchable Strain Sensor for Human–Machine Interfaces Comprising a Nanohybrid of Carbon Nanotubes and Conductive Elastomers

Eun Roh,[†] Byeong-Ung Hwang,[‡] Doil Kim,[‡] Bo-Yeong Kim,[†] and Nae-Eung Lee*[,†,‡,§]

[†]SKKU Advanced Institute of Nanotechnology (SAINT), [‡]School of Advanced Materials Science & Engineering, and [§]Samsung Advanced Institute for Health Sciences & Technology (SAIHST), Sungkyunkwan University (SKKU), Suwon, Kyunggi-do 440-746, Korea

ABSTRACT Interactivity between humans and smart systems, including wearable, body-attachable, or implantable platforms, can be enhanced by realization of multifunctional human–machine interfaces, where a variety of sensors collect information about the surrounding environment, intentions, or physiological conditions of the human to which they are attached. Here, we describe a stretchable, transparent, ultrasensitive, and patchable strain sensor that is made of a novel sandwich-like stacked piezoresistive nanohybrid film of single-wall carbon nanotubes (SWCNTs) and a conductive elastomeric composite of polyurethane (PU)-poly(3,4-ethylenedioxythiophene) polystyrenesulfonate (PEDOT:PSS). This sensor, which can detect small strains on human skin, was created using environmentally benign water-based solution processing. We attributed the tunability of strain sensitivity (*i.e.*, gauge factor), stability, and optical transparency to enhanced formation of percolating networks between conductive SWCNTs and PEDOT phases at interfaces in the stacked PU-PEDOT:PSS/SWCNT/PU-PEDOT:PSS structure. The mechanical stability, high stretchability of up to 100%, optical transparency of 62%, and gauge factor of 62 suggested that when attached to the skin of the face, this sensor would be able to detect small strains induced by emotional expressions such as laughing and crying, as well as eye movement, and we confirmed this experimentally.

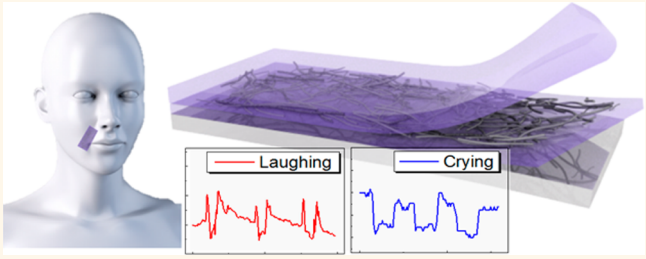

KEYWORDS: stretchable electronics · transparent electronics · strain sensor · single-wall carbon nanotube · human monitoring

For effective interactions between humans and smart systems in pervasive computing environments, human–machine interfaces that can detect the surrounding environment, physical activities, health status, intentions, and emotions of humans and send the monitored data are required.[1−7] This can be achieved by human–machine interfaces integrated in smart systems such as smart home appliances, robots, drones, phones, tablets, watches, bands, contact lenses, glasses, patches, and pacemakers as stand-alone, mobile, portable, wearable, patchable, or implantable platforms. The requirement for future smart human–machine interfaces to have interactivity capabilities resembling human modalities necessitates a myriad of sensors with functions optimized for specific platforms and applications. The advent of new wearable, patchable, or implantable platforms, in particular, requires functionalities such as flexibility, stretchability, stability, and/or optical transparency.

Detection of strains induced on human skin using patchable conformal strain sensors is one approach to monitor human emotions,[8] intentions, and activities.[2,9,10] Even though stand-alone vision sensors are generally used to detect movement of the human body[11,12] and analyze facial expression changes due to emotion,[13] vision systems have low mobility and high complexity, are expensive, and are difficult to adapt to wearable, patchable, or implantable electronics. As an alternative approach,

* Address correspondence to nelee@skku.edu.

Received for review March 16, 2015 and accepted April 13, 2015.

Published online April 13, 2015
10.1021/acsnano.5b01613

on-body patchable strain sensors can be used to detect various ranges of strain induced on human skin in an unobtrusive way. Stretchable conformal strain sensors attached to the skin near the joints of fingers,[1,14−22] hands,[11,14,23−26] and knees[1,22,27] can detect large strains induced by movements such as walking, running, and grasping. To detect large strains, the strain sensor should have large stretchability, similar to a goniometer. In addition to large strain, detection of small strains on the skin of the face,[26,28] eyes,[26] or neck[1,19,25,26] can also be used to monitor the normal daily activities of a human. In this case, the strain sensor needs to have sufficiently high sensitivity to detect variations in strain of a few percentage points or below, in contrast to strain sensors for detecting large strains, and needs to be stretchable to make conformal contact with the skin with high signal quality.

Stretchable conformal strain sensors have been developed from highly stretchable piezoresistive materials because of simplicity of design, low cost, ease of fabrication, and high sensitivity (*i.e.*, gauge factor).[3,29] The gauge factor, GF, is defined as GF = $(\Delta R/R_0)/\varepsilon$, where ΔR is the resistance change with straining, R_0 the resistance before straining, and ε the applied strain. Most stretchable strain sensors based on metallic conductors[14,16,25] or the nanomaterials of carbon nanotubes (CNTs)[1,21,30,31] and graphene[15,17,32,33] have a GF value less than 15 (see Table S1 in the Supporting Information). One of the common approaches to obtain high piezoresitivity as well as stretchability in piezoresistive elastomeric materials is to fill the elastomeric matrix with conductive nanofillers to obtain a percolating network that serves as a conduction path.[18−20] For example, stretchable strain sensors based on elastomeric composites of CNTs,[27,34,35] silver nanowires (AgNWs),[18] graphene,[19] and carbon black[20,24,36,37] showed improved GF values and stretchability (Supporting Table S1). To detect very small skin strains, however, elastomeric piezoresisitve materials with both high GF and stretchability are required.

An important feature for widespread user acceptance of conformal strain sensors on areas of the human body such as the face and neck is optical transparency so that the sensor is invisible during daily activities. Most reported conformal stretchable strain sensors are nontransparent because of high loading of nontransparent inorganic nanofillers (see also Table S1). Optical transparency of stretchable sensors also enables the integration of optical components.[3,38] However, few transparent and stretchable strain sensors with high strain sensitivity have been reported.

Herein, we report transparent, stretchable, ultrasensitive, and tunable strain sensors made of a novel stacked nanohybrid structure of single-wall CNTs (SWCNTs) and a conductive elastomer of poly(3,4-ethylenedioxythiophene) (PEDOT:PSS) and a polyurethane (PU) dispersion. The three-layer stacked and sandwich-like nanohybrid of PU-PEDOT:PSS/SWCNT/PU-PEDOT:PSS in sequence provides tunability of stretchability, optical transparency, strain sensitivity, and stability. Stacking of the organic-based layers was possible using an environmentally friendly, water-soluble solution. The low concentration of SWCNTs resulted in high optical transparency, while the conductivity and sensitivity of the sensor were easily tuned by using a conductive elastomer instead of a nonconductive elastomer, resulting in increased percolation between SWCNTs and PEDOT phases at the interfaces between layers. A transparent and stretchable strain sensor with an optical transparency of 63%, GF of 62.3, and stretchability above 100% was tested for stable detection of skin strains. This sensor still worked well even after 1000 stretching cycles at 20% strain. We demonstrated that this strain sensor could detect small strains on the skin of a human face induced by minute movements of muscles related to facial expressions caused by emotions and eyeball movements. We attributed the detectability of emotional expressions by the stretchable and transparent strain sensor to the ultrahigh sensitivity of the sensor. The transparent and stretchable sensor described here has great potential and will add value to wearable or patchable smart systems.

RESULTS AND DISCUSSION

A schematic illustration of stretchable, transparent, and ultrasensitive strain sensors attached to the forehead, near the mouth, under the eye, and on the neck to sense skin strains induced by muscle movements during expression of emotion and daily activities is presented in Figure 1a. A cross-sectional schematic of the strain sensor showing the stacked sandwich-like structure of SWCNTs and conductive PU-PEDOT:PSS composite elastomer on a PDMS substrate is shown in Figure 1b. The three-layer stacked nanohybrid strain sensor had improved stability in sensor responses compared to that of single-layer (SWCNT or conductive composite elastomer) or two-layer (SWCNT(top)/PU-PEDOT:PSS (bottom) and *vice versa*) sensors. Different layer designs are discussed later. Details of the materials and processes used to fabricate the sensors are provided in the Methods section and Supporting Information (Figure S1). Briefly, a thin and stretchable polydimethylsiloxane (PDMS) substrate treated by oxygen plasma was spin-coated with a water-soluble PU-PEDOT:PSS composite solution. It is important to use a water dispersion of PU for uniform distribution of the conductive polymer phase in the elastomeric composite conductor based on a water-based PEDOT:PSS solution. After spin-coating of the bottom conductive PU-PEDOT:PSS composite elastomer (~100 nm in thickness) on the PDMS substrate, the surface of the bottom composite layer was functionalized with 3-aminopropyltriethoxysilane (APTES) solution to form

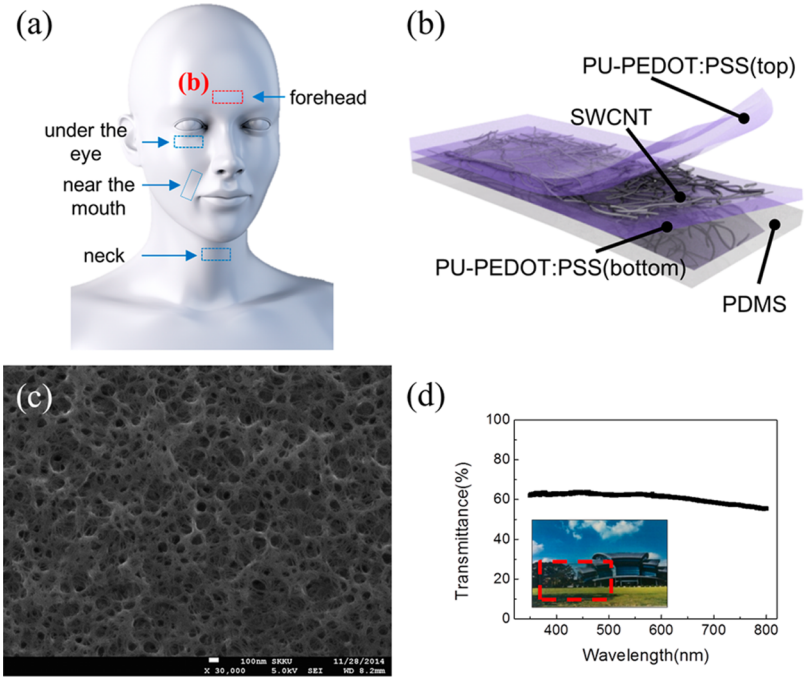

Figure 1. (a) Schematic illustration of stretchable transparent ultrasensitive strain sensors attached to the forehead, near the mouth, under the eye, and on the neck to sense skin strains induced by muscle movements during expression of emotions and daily activities. (b) Schematic illustration of the cross-section of the strain sensor consisting of the three-layer stacked nanohybrid structure of PU-PEDOT:PSS/SWCNT/PU-PEDOT:PSS on a PDMS substrate. (c) Top-view FE-SEM image of the three-layer stacked nanohybrid sensor. (d) Transmittance spectra of the three-layer stacked nanohybrid sensor in the visible wavelength range from 350 to 700 nm. A photograph of the sensor is shown as an inset.

amino groups for good adhesion with the SWCNT layer. A water-based solution with different concentrations of SWCNTs was dropped over the functionalized PU-PEDOT:PSS surface, followed by a 10 min incubation, and then droplets were spread out uniformly by spin coating. After annealing the SWCNT layer for 1 h at 100 °C, SWCNTs at the bottom PU-PEDOT:PSS layer surface were functionalized using APTES solution, and then the top PU-PEDOT:PSS solution was spin-coated.

Before verifying the sensing characteristics of the fabricated sensors, the surface morphologies of coated conducting elastomeric composite and SWCNTs were investigated. Figure 1c shows a top-view FE-SEM image of a three-layer stacked nanohybrid sensor (PU-PEDOT:PSS (top)/SWCNT/PU-PEDOT:PSS (bottom)) and surface morphologies of the PU-PEDOT:PSS layer. Here, the composition and thickness of the PU-PEDOT:PSS composite elastomer was 60−40% and 100 nm, respectively. The layer coated with a 5 mg/mL SWCNT solution was sandwiched between the two conductive elastomers. The image in Figure 1c shows that the surface of the sensor structure appeared porous due to interaction with SWCNTs and both sides of the bottom and top conductive elastomer layers. To gain further insight into the observed surface morphology of the different stacked structures, PU-PEDOT:PSS, SWCNT, and SWCNT/PU-PEDOT:PSS layers were coated on a Si wafer, and top-view FE-SEM images of them were taken (Supporting Figure S2a,b,c, respectively). The composition and thickness of the elastomeric composite and conditions used to coat the SWCNTs were the same as those used to fabricate the sensor shown in Figure 1c. The surface morphology of PU-PEDOT:PSS indicated that the solution of PU-PEDOT:PSS was composited well with no aggregation (Figure S2a). The surface morphology of the water-based SWCNT film on the Si wafer indicated the formation of fibrils of SWCNTs (Figure S2b). The FE-SEM image of SWCNTs coated on the bottom PU-PEDOT:PSS composite layer (Figure S2c) showed that the SWCNTs were embedded slightly in the bottom PU-PEDOT:PSS layer after coating and thermal annealing. When the SWCNT layer coated on the elastomer composite layer is annealed at an elevated temperature of 100 °C near or above the glass transition temperature (T_g) of PU (60−120 °C),[39] interaction between SWCNTs and highly viscoelastic PU may cause embedding of SWCNTs. SWCNTs were therefore slightly embedded and fixed at the soft bottom layer of PU-PEDOT:PSS during annealing at an elevated temperature. To fabricate a sandwich-like structure, PU-PEDOT:PSS was coated on the surface of SWCNTs as a top layer. The top PU-PEDOT:PSS layer covering the SWCNTs embedded in the bottom PU-PEDOT:PSS layer had a porous-like surface morphology, presumably because the top PU-PEDOT:PSS layer followed the topographic features of the SWCNT layer surface. The top of the sandwich-like sensor structure (PU-PEDOT:PSS/SWCNT/PU-PEDOT:PSS), therefore, had

a porous surface. On the basis of the surface morphologies of the different film structures (Figure S2a,b,c), we attributed the porous-like surface of the sensor observed in Figure 1c to embedding of SWCNTs into the bottom PU-PEDOT:PSS layer caused by a decrease in the T_g of PU and removal of water as a solvent during annealing of the top PU-PEDOT:PSS layer. The fabricated sensor with a sandwich-like stacked structure prepared with 5 mg/mL SWCNT solution showed the optical transmittance of 62% in the visible range, which provides optical transparency enough for an aesthetic view of the human body (Figure 1d).

To investigate the role of SWCNTs in electrical transport, we measured the current with an applied voltage of 0 to 1 V. The data in Supporting Figure S2d show electrical currents through the different films of PU-PEDOT:PSS, SWCNT, and stacked PU-PEDOT:PSS (bottom)/SWCNT (top). As seen in Figure S2d, the current that flowed through SWCNTs embedded in the PU-PEDOT:PSS layer was much higher than the current that flowed through only the PU-PEDOT:PSS or SWCNT layers. These data indicate that interaction of SWCNTs and PU-PEDOT:PSS in the stacked structure resulted in more effective electrical transport. When SWCNTs are slightly embedded in the PU-PEDOT:PSS layer, SWCNTs and PEDOT:PSS are electrically connected because PEDOT:PSS, which is composed of PEDOT phases (conducting area) in the PSS gel state (insulating area), forms junctions with the SWCNT nanofillers.[40] Therefore, enhanced connectivity between PEDOT phases and SWCNTs induced much higher electrical conductivity in the stacked PU-PEDOT:PSS/SWCNT layer.

To optimize the performance of the sensor with the sandwich structure of PU-PEDOT:PSS/SWCNT/PU-PEDOT:PSS, we compared other configurations using PU, PEDOT:PSS, and SWCNT in Figure S3 in the Supporting Information. The responses of each layer coated on the PDMS substrate to strain under cyclic bending tests were tested and compared. The $\Delta R/R_0$ responses of PU-PEDOT:PSS, SWCNT, and SWCNT layers with PU encapsulation measured under cyclic bending are shown in Figure S3a,b,c, respectively. The PU-PEDOT:PSS layer with a ratio of 60−40 (wt %) that is composed of a PU matrix and uniformly distributed PEDOT:PSS showed very similar response signals at the different strains (Figure S3a). In contrast, the SWCNT single layer had a much higher sensitivity, but its electrical response showed poor stability (Figure S3b). When the SWCNT layer was covered with a PU layer, the sensitivity was decreased due to suppression of the movement of SWCNTs, but the stability of the signal response was much higher (Figure S3c). Figure S3d and e show the strain responses of the stacked layers of PU-PEDOT:PSS (bottom)/SWCNT/PU (top) and PU (bottom)/SWCNT/PU-PEDOT:PSS (top), respectively. Higher sensitivity with good stability was observed for the sandwich-like PU (bottom)/SWCNT/PU-PEDOT:PSS (top) structure than the PU-PEDOT:PSS (bottom)/SWCNT/PU (top) structure. In the case of the PU-PEDOT:PSS (bottom)/SWCNT/PU (top) structure, the electrical path though slightly embedded SWCNTs into the bottom PU-PEDOT:PSS elastomeric conducting layer under strain was less strongly affected, which increased the stability of the PEDOT:PSS (bottom)/SWCNT/PU (top) to strain. Sensitivity, which is determined by the contact area of PEDOT:PSS with SWCNTs, was low because a smaller number of embedded SWCNTs contacted the conductive PEDOT phases in the PU-PEDOT:PSS layer; the rest of the SWCNTs were in contact with the insulating top PU layer (Figure S3d). In the PU (bottom)/SWCNT/PU-PEDOT:PSS (top) structure, SWCNTs were slightly embedded and fixed at the bottom PU layer, and the top PU-PEDOT:PSS layer covered the surface of the stacked SWCNTs. Even though the electrical current flowed through the SWCNTs with PEDOT:PSS due to connection of PEDOT phases as a conducting area by SWCNTs before strain was applied, the current path was broken, and it was hard for the current to flow due to movement of SWCNTs under applied strain. In other words, a large change in the resistance resulted in high sensitivity (Figure S3e). Figure S3f shows the GF values obtained for different films at different strains. The highest GF of 109 was obtained at the strain of 2.5% for the SWCNT layer, but the stability of the response signal was very poor. On the basis of the data shown in Figure S3, we concluded that the stability of sensor responses was affected mainly by SWCNTs embedded in the bottom layer due to a decrease in T_g of the underlayer and the top conductive elastomer layer, while the sensitivity of the stacked nanohybrid strain sensor was primarily determined by the formation of electrical junctions between SWCNTs and PEDOT phases in the PU-PEDOT:PSS composite. Use of the sandwich-like stacked structure of SWCNTs and conductive elastomeric composites provides a viable strategy for obtaining a large strain sensitivity by the large modulation of percolation electrical transport through electrical junctions between SWCNTs and PEDOT phases and at the same time an improved stability in the sensing signal due to mechanical holding of SWCNTs by the bottom and upper elastomeric conductors. On the basis of the results obtained from comparative studies, we chose the PU-PEDOT:PSS (bottom)/SWNCT/PU-PEDOT:PSS (top) structure with the highest sensitivity and stability for the sensor structure.

We next evaluated different SWCNT concentrations for SWCNT layer formation in PU-PEDOT:PSS (bottom)/SWCNT/PU-PEDOT:PSS (top) to fabricate a sensor with optical transparency. Figure 2a, b, and c show the measured time-dependent normalized resistance change ($\Delta R/R_0$) of three-layer stacked nanohybrid sensors with SWCNT concentrations of 1, 3, and 5 mg/mL,

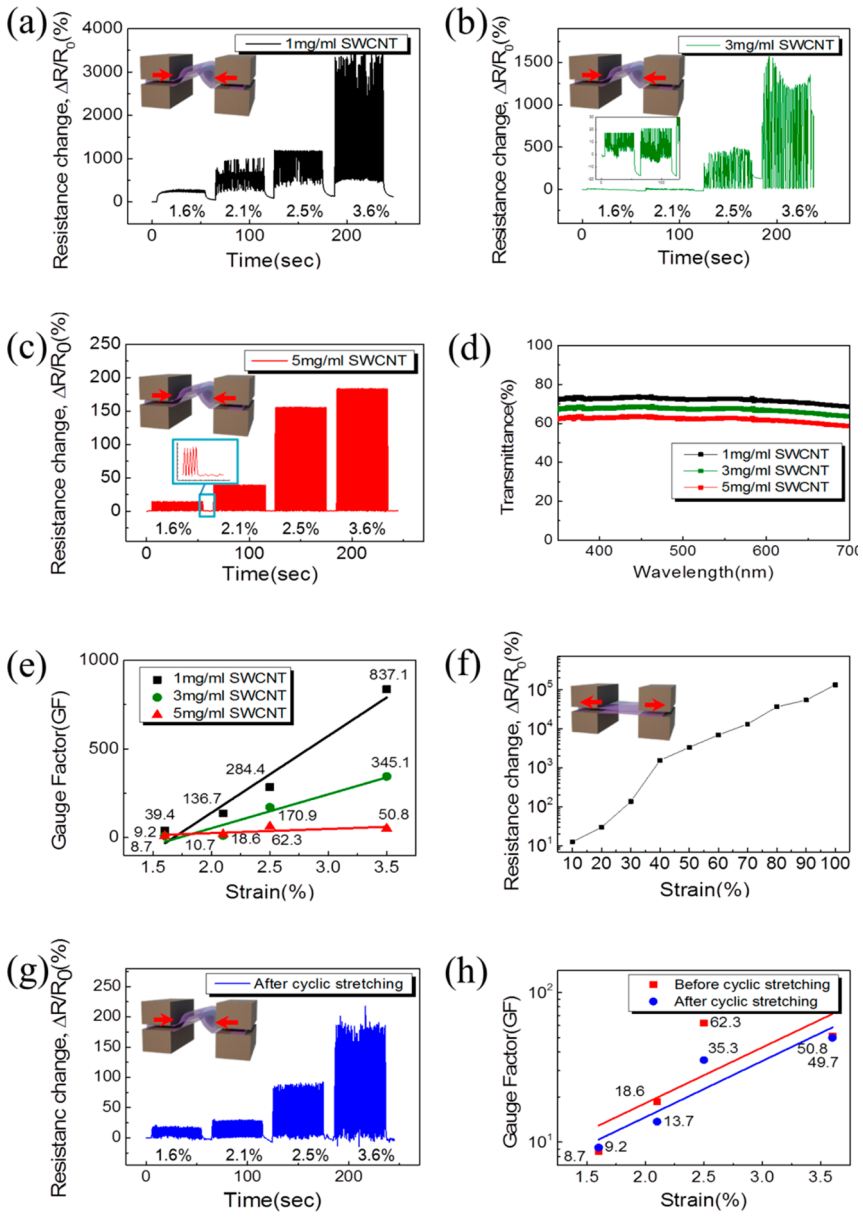

Figure 2. Time-dependent normalized resistance changes ($\Delta R/R_0$) of the three-layer stacked nanohybrid strain sensor with SWCNT concentrations of (a) 1, (b) 3, and (c) 5 mg/mL under strains of 1.6%, 2.1%, 2.5%, and 3.6% in response to repetitive bending cycles (50 cycles per strain). The ratio of PU-PEDOT:PSS was 60:40 (wt %). (d) Optical transmittance of three-layer stacked sensors with SWCNT concentrations of 1, 3, and 5 mg/mL in the visible range from 350 to 700 nm. (e) Gauge factor of the sensors based on SWCNT concentrations of 1, 3, and 5 mg/mL and the bottom PU-PEDOT:PSS layer according to strain. (f) Strain-dependent $\Delta R/R_0$ of the sensor at stretching strains ranging from 10% to 100%. (g) Time-dependent $\Delta R/R_0$ of the sensor in response to strains of 1.6%, 2.1%, 2.5%, and 3.6% with repetitive bending cycles (50 cycles per strain) after 1000 repetitive stretching cycles up to 20% strain. (h) Gauge factor of the sensors before and after cyclic stretching *versus* bending strain.

respectively, under cyclic bending in a small strain range. Each sensor was subjected to strains of 1.6%, 2.1%, 2.5%, and 3.6% with 50 bending cycles at each strain. The SWCNT concentration significantly affected the electrical responses toward different bending strains. The sensor based on 1 mg/mL SWCNTs had an extremely high sensitivity but poor stability (Figure 2a). The sensitivity of the sensor based on 3 mg/mL SWCNTs was slightly decreased relative to that of the 1 mg/mL SWCNT sensor, but its response stability was poor (Figure 2b). The sensor based on 5 mg/mL SWCNTs had outstanding stability, but slightly lower sensitivity in the higher strain range than the other sensors evaluated (Figure 2c). The increase in stability and decrease in sensitivity with increasing concentration of SWNCTs is due to changes in the level of electrical transport depending on the average distance between SWCNTs and the number of SWCNTs connected with the PEDOT phases in the composite elastomer. Increasing the concentration of SWCNTs resulted in increased contact with PEDOT:PSS, which increased current flow. Therefore, increased contact

area between SWCNTs and PEDOT:PSS increased conductance and, in turn, relative resistance; that is, the sensitivity decreased with higher SWCNT loading. However, more junctions between SWCNTs and PU-PEDOT:PSS were maintained under straining during bending, which enhanced the stability of those sensors with higher concentrations of SWCNTs. Sensors fabricated with 1, 3, and 5 mg/mL of SWCNTs had optical transmittance values of 72%, 67%, and 63%, respectively, in the visible range from 350 to 700 nm (Figure 2d). At higher concentrations of SWCNTs, a high loading of SWCNTs made the sensors less transparent. Figure 2e shows the GF values of sensors with different concentrations of SWCNTs obtained from the data in Figure 2a,b,c. The GF value of the sensor with 1 mg/mL SWCNTs was much higher than those of sensors with other concentrations of SWCNTs. Even though the 1 mg/mL SWCNT sensor had high sensitivity and a GF value up to 837.1 under the 3.5% strain, the 5 mg/mL SWCNT sensor had a GF as high as 62.3 under the 2.5% strain. The time-dependent $\Delta R/R_0$ responses of the stretchable sensor fabricated with 5 mg/mL SWCNTs under stretching in the strain range from 10% to 100% were measured, and the data are shown in Figure 2f. We confirmed the operation capability of the sensor up to 100%. For comparison, stretchability of the PU-PEDOT:PSS layer and SWCNT (top)/PU-PEDOT:PSS (bottom) structure was also measured in the stretched state under strains ranging from 10% to 100%; these data are shown in Figure S4. The three-layer stacked structure had a higher sensitivity under increased strain during the stretching test than the other structures evaluated. In the case of the PU-PEDOT:PSS single layer with no nanofillers, the film shows low responsivity to strain due to the absence of movement of nanofillers. The sensitivity of the PU-PEDOT:PSS (bottom)/SWCNT (top) structure was higher than that of the PU-PEDOT:PSS single layer due to SWCNTs embedded into the bottom layer, but lower than that of the stacked PU-PEDOT:PSS (bottom)/SWCNT/PU-PEDOT:PSS (top) structure because of the smaller contact area between SWCNTs and PEDOT:PSS. In addition, the time-dependent $\Delta R/R_0$ responses of the three different structures were also measured at repetitive stretching cycles under strains ranging from 10% to 30% (Figure S4b,c,d). Larger responsitivity was observed for the sensor with the PU-PEDOT:PSS (bottom)/SWCNT/PU-PEDOT:PSS (top) structure than the PU-PEDOT:PSS single layer and PU-PEDOT:PSS (bottom)/SWCNT (top) structure. These results indicate that the stretchable and transparent strain sensor with a novel three-layer stacked PU-PEDOT:PSS (bottom)/SWCNT/PU-PEDOT:PSS (top) structure described in this study can detect large-scale strains in the stretching mode. However, comparing the data in Figures 2c and S4b, obtained from the same sensor structure, a large difference was observed in the $\Delta R/R_0$ data, for example, ~150% under 2.5% bending strain (Figure 2c) and ~10% under 10% stretching strain (Figure S4b), because under a large strain fractured and deformed SWCNTs make the sensor response hard to recover. This phenomenon can be explained by an increased baseline signal observed in Figure S4b. In addition, strain-dependent $\Delta R/R_0$ data of PU-PEDOT:PSS layers with the different ratios of 80:20, 60:40, and 20:80 (wt %) were obtained and compared under stretching modes (Figure S4e). The PU-PEDOT:PSS layer with the ratio of 60:40 shows higher strain responsivity compared to the other layers with other composition ratios.

To verify the durability and reproducibility of the strain sensor after repetitive cyclic stretching, sensor responses to small bending strains were measured after repetitive stretching of 1000 cycles up to 20%. The sensor after cyclical stretching still maintained an electrical performance (high stability and high sensitivity) similar to that before the cyclic stretching tests (Figure 2g). Even though the GF value decreased slightly compared to the initial value before cyclic stretching, the GF values of the cyclically stretched sensor were 9.2, 13.7, 35.3, and 49.7 under strains of 1.6%, 2.1%, 2.5%, and 3.6%, respectively (Figure 2e).

We next evaluated the ability of the sensor to detect human activities. Recognition of human emotions is critical in the human monitoring field.[41] Eye movements, wrinkling of the forehead, and many other expressions can indicate intentions and the physiological state of humans.[42] To investigate the ability of the sensor to function as an emotion detector, sensors were attached to the forehead and skin near the mouth of a subject, and sensor responses were monitored (Figure 1a). Time-dependent $\Delta R/R_0$ responses of the sensors attached to the forehead and skin near the mouth when the subject was laughing are shown in Figure 3a and b, respectively. While the highest peak of the $\Delta R/R_0$ from the sensor on the forehead was 0.6% (Figure 3a), the highest peak of the $\Delta R/R_0$ from the sensor on the skin near the mouth was 40% (Figure 3b). The difference in peak $\Delta R/R_0$ values is due to differences in the degree of muscle movements. In general, when a person smiles or laughs, the muscles around the mouth and cheekbone make larger movement than in other facial areas. Muscles around the forehead, frontalis, or temporoparietalis move only slightly. Expression of sadness, in contrast, results in larger movements of muscles around the forehead.[43] Figure 3c and d show the $\Delta R/R_0$ responses of a sensor attached to the forehead and near the mouth, respectively, when the subject was crying. The highest peak in the $\Delta R/R_0$ response of the sensor on the forehead was almost 200% (Figure 3c), while the highest peak in the $\Delta R/R_0$ response of the sensor on the skin near the mouth was slightly over 0% (Figure 3d). The different responses of the sensors on the forehead and skin near the mouth

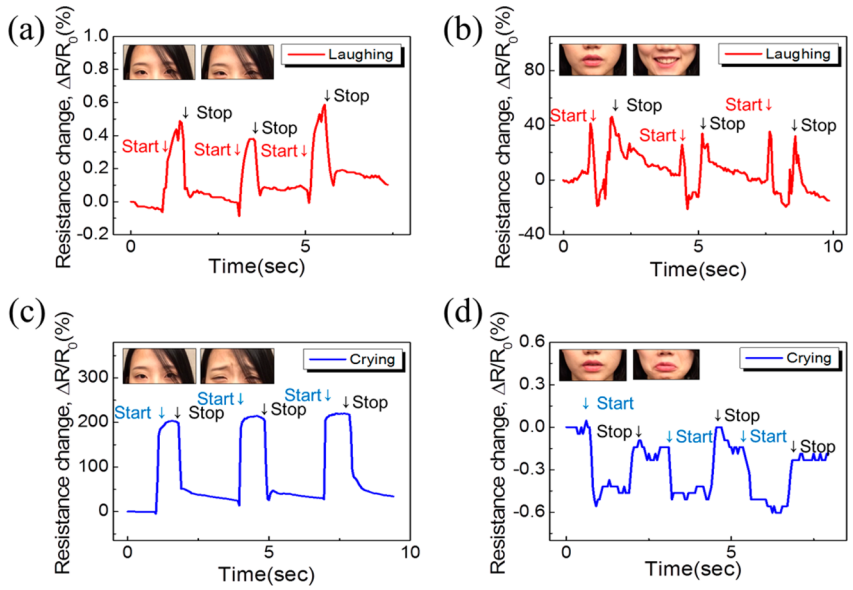

Figure 3. Time-dependent $\Delta R/R_0$ responses of the sensor attached to the (a) forehead and (b) skin near the mouth when the subject was laughing and of the sensor attached on the (c) forehead and (d) skin near the mouth when the subject was crying.

enable differentiation between the emotions of joy and sadness. Figure S5 shows the $\Delta R/R_0$ responses of the sensor attached to the skin around the temporal muscle and the skin under the eye when the subject was laughing or crying. The $\Delta R/R_0$ signal peaks were not markedly different (~1% difference) because the temporal muscles and those under the eyes are not involved in laughing or crying. For detection of a small-scale strain distribution on the skin induced by simultaneous movements of multiple muscles, a strain sensor array with much improved conformal contact with the skin may distinguish subtle differences in the distributed strains. For improved conformal contact of the stretchable sensor with human skin, dry adhesive structures on the surface of thinner substrates, such as microhairy patterns,[44] need to be employed.

To obtain more detailed sensor responses, we measured the ability of sensors attached to the skin under the eye to detect emotion or intention (Figure 1a). The ability of the sensors to detect eye blinking and movements was monitored. Detection of eye movements refers to the ability to sense sizing, vibrating, blinking, or rolling of the eyeballs. Even though facial muscle movement can be detected by visual methods, eye movement is too difficult to detect using a camera or by eye due to the minuteness of the movements. However, blinking and eyeball rolling could potentially be measured by a stretchable, transparent, ultrasensitive strain sensor attached to the skin under the eye. Figure 4a shows the $\Delta R/R_0$ responses of a sensor attached to the skin under the left eye when the subject was blinking. The peak $\Delta R/R_0$ signal increased up to 2% with good stability. Figure 4b and c show the $\Delta R/R_0$ responses of the sensor when the subject looked right and left, respectively. When the eyeballs moved from the center to the right and then to the center, the $\Delta R/R_0$ response decreased and then increased again (Figure 4b). In contrast, when the eyeballs moved from the center to the left and then to the center, the $\Delta R/R_0$ response increased and then decreased again (Figure 4c). The observed opposite tendency in the $\Delta R/R_0$ response was caused by opposite movement of eye muscles. Each eye is surrounded by six muscles—the lateral rectus, medial rectus, superior rectus, inferior rectus, inferior oblique, and superior oblique—and these muscles move differently depending on the direction of the gaze. When a person looks right, the lateral rectus surrounding the right side section of the eye contracts, but the medial rectus surrounding the left section of the eye stretches. In contrast, when a person looks left, the medial rectus surrounding the left section of the eye contracts, but the lateral rectus at the opposite side stretches. Figure 4d and e show the $\Delta R/R_0$ responses of the sensor when the subject looked up and down, respectively. When the eyeball moved upward from the center, the $\Delta R/R_0$ increased (Figure 4d). When the eyeball moved downward from the center, the $\Delta R/R_0$ decreased (Figure 4e). This phenomenon can also be explained by opposite movement of muscles: the superior rectus stretched when the subject looked down and contracted when the person looked up, while the inferior rectus contracted when the person looked down and stretched when the person looked up. Strains induced by eye movements were detected and distinguished easily using a stretchable conformal strain sensor attached to the face, indicating that these sensors are appropriate for application in emotion analysis and human–machine interface technology. Multiple strain sensors attached to various areas near the eye

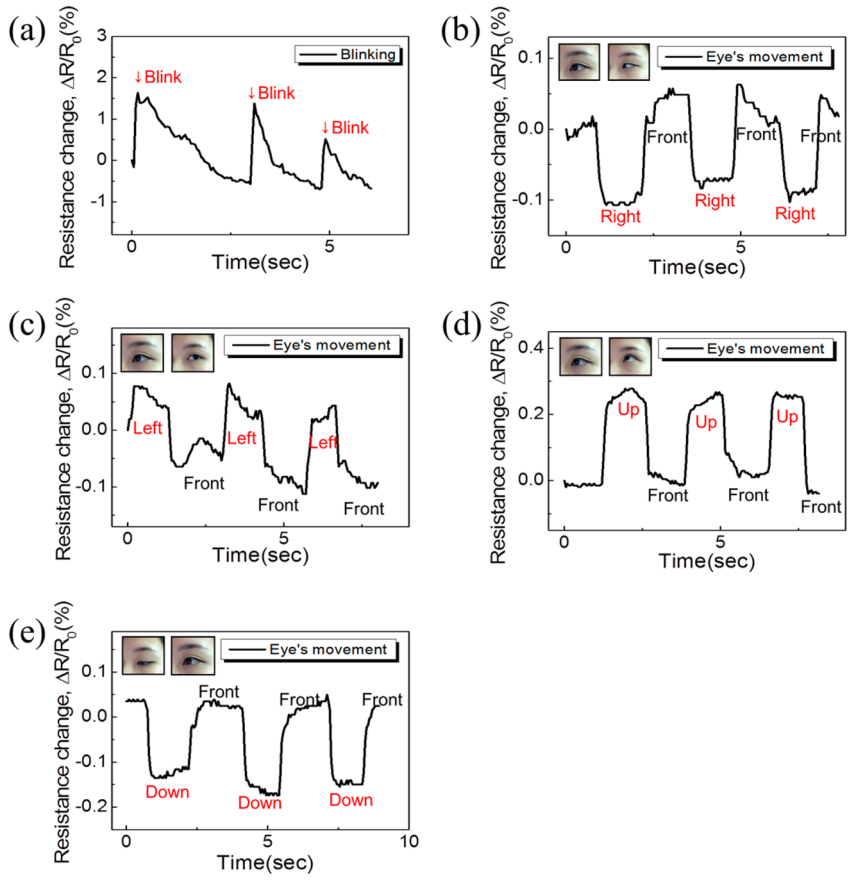

Figure 4. Time-dependent $\Delta R/R_0$ responses of a sensor attached under the eye (b) when a subject was blinking and when the subject was looking (c) right, (d) left, (e) up, and (f) down.

may provide distinctive and simultaneous detection of the different eye movements.

We also evaluated the ability of the sensor to respond to other motions such as breathing, swallowing, and speaking by attaching the sensor to the neck. Measured sensor responses are shown in Figure S6. We also identified high responsivity of the sensor with high stability to muscle movements of the trachea and esophagus in the neck. Additionally, we repetitively measured the $\Delta R/R_0$ using the same sensor attached to and detached from the same forehead three times to confirm the repeatability of the sensor in repetitive measurements (Figure S7). The data in Figure S7 indicate that the sensor signals were nearly unchanged after repetitive attachment and detachment.

To verify the durability and reproducibility of the sensor after repetitive stretching cycles at strains of 20% and 30%, we evaluated the responsivity of the sensor to human skin strains caused by muscle movements during laughing and crying; the data are shown in Figures S8 and S9, respectively. In the case of laughing, the highest peak in the $\Delta R/R_0$ from the sensor attached to the forehead was almost 10% (Figure S8a), whereas the highest peak in the $\Delta R/R_0$ response from the sensor attached to the skin near the mouth was almost 80% (Figure S8b). When the subject was crying, the highest peak of $\Delta R/R_0$ from the sensor attached to the forehead was almost 40% (Figure S8c), while the highest peak of the $\Delta R/R_0$ response from the sensor attached to the skin near the mouth was 15% (Figure S8d). Figure S8e, f, g, and h show the $\Delta R/R_0$ responses from the sensor attached to the skin under the left eye when the subject looked right, left, up, and down, respectively; the peaks of the $\Delta R/R_0$ responses were almost 1%. When the eyeball moved from the center to the right and then to the center, the $\Delta R/R_0$ response decreased and then increased again (Figure S8e). In contrast, when the eyeball moved from the center to left and then to the center, the $\Delta R/R_0$ response increased and then decreased again (Figure S8f). When the eyeball moved upward from the center, the $\Delta R/R_0$ increased (Figure S8g), and when the eyeball moved downward from the center, the $\Delta R/R_0$ decreased (Figure S8h). The results shown in Figure S8 indicate that the sensors had sufficient durability under cyclic stretching at 20% strain. Even though the electrical responses of the sensor after 1000 repetitive stretching cycles at a strain of 30% showed low stability, the responsivity of the sensor to laughing and crying and eye movements remained outstanding (see details in Supporting Figure S9).

CONCLUSIONS

In summary, we fabricated a transparent, stretchable, and highly sensitive strain sensor with the novel stacked nanohybrid structure of PU-PEDOT:PSS/SWCNT/PU-PEDOT:PSS and tunable electrical and optical properties. All materials were based on water as the solvent, which made the fabrication process environment friendly and easy to control. The electrical responses of the sensor to bending and stretching strains were assessed using a cyclic and static straining measurement system because a stretchable conformal strain sensor has to have high stability and sensitivity. The application of 1000 cyclic stretching tests under strains of 20% to 30% did not change the intrinsic properties of the sensor. We attribute the high stability of the sensor to the top and bottom conducting elastomer layers in the sandwich-like structure, where movements of SWCNTs embedded into the bottom PU-PEDOT:PSS layer are mechanically stable. We ascribe the high sensitivity of the sensor to the interaction of SWNCTs with the PU-PEDOT:PSS elastomeric conductor in a sandwich-like structure where the SWCNTs function as a bridge that connect the conductive PEDOT to the PEDOT phases. Insertion of a SWCNT layer between the PU-PEDOT:PSS layers makes electrical transport more effective and increases strain responsivity.

We also demonstrated that the transparent, stretchable, and highly sensitive sensors could detect emotional expressions and eye movements; in particular, the sensors could detect and distinguish between the emotions of laughing and crying. Moreover, the sensors could distinguish between eye movements in different directions, which the human eye or a visual camera cannot do. Therefore, the patchable strain sensor presented here can be applied to not only sensing various emotions but also various fields such as personal health care and human–machine interfaces. In addition, integration of the arrayed strain sensors with various other sensors that detect skin temperature, sweat, heartbeat, *etc.,* will provide more detailed emotion detection and be an important research subject in the future.

METHODS

Materials. Single-walled carbon nanotube powder functionalized with carboxylic groups (–COOH) was purchased from UniNanoTech Co., Ltd. The mean length and diameter of COOH-functionalized SWCNTs was 18 μm and 2 nm, respectively. To fabricate water-based SWCNT solutions with different concentrations, 10, 30, and 50 mg of SWCNT powder was mixed with 10 mL of deionized water with 0.1 mL of polystyrenesulfonate (PSS) solution followed by sonication for 30 min.

Preparation of Polymer Solution Blend. A 40 wt % PU dispersion solution (Alberdingk U3251 from Alberdingk Boley) was diluted with distilled water to 1 and 4 wt % PEDOT:PSS solutions (CLEVIOS PH1000 from Heraues) and mixed with 5–8 wt % dimethyl sulfoxide (Sigma-Aldrich) and 1 wt % Zonyl FS-300 (Sigma-Aldrich). After that, 4 mL of PEDOT:PSS solution was dropped by syringe pump into the 6 mL PU solution.

Fabrication of Stretchable and Transparent Strain Sensors. Stretchable and transparent strain sensors were fabricated as follows. Using a PDMS elastomer kit (Sylgard 184 from Dow Corning), 500 μm thick PDMS 2 $\times$ 4 cm^2 in size was fabricated as a substrate for the sensor. After treatment of the PDMS surface with O_2 plasma to make the surface hydrophilic, a 100 nm thick PU-PEDOT:PSS composite elastomer layer comprising PU (60 wt %) and PEDOT:PSS (40 wt %) was deposited on the substrate by spin-coating for 5 s. After annealing at 150 °C for 1 h, the composite film surface was treated as a self-assembled monolayer (SAM) by a (3-aminopropyl)triethoxysilane solution (741442 from Sigma-Aldrich) for 30 min to obtain a water-based SWCNT solution coated on the plasma-treated PDMS substrate. After SAM treatment, the water-based SWCNT solution was dropped on the surface for 10 min and the solution was coated uniformly (1.2 μm thickness) using a spin-coater at a spinning speed of 1000 rpm. For thermal annealing, the sample was heated at 100 °C for 1 h and water was removed. After annealing, the PU/PEDOT:PSS solution was coated on the SWCNT surface again after SAM treatment. Then, the device was annealed at 100 °C for 1 h.

Characterization of the Stretchable and Transparent Strain Sensor. Repetitive bending and stretching tests were carried out using Au–Ni woven conductive textiles (Silverized Nylon/Spandex Knit SMP 130, Solueta Co. Ltd.) as electrodes for electrical contact without damage to the sensor in a custom-made bending/stretching system. To detect the emotion of a subject and eye movements, the fabricated sensors were attached to the face skin using double-sided tape. Copper wires were used to connect the sensor attached to the human face with silver paste to an analyzer (HP4145B, Agilent Technologies) to detect facial expressions.

Conflict of Interest: The authors declare no competing financial interest.

Acknowledgment. This research was supported by the Basic Science Research Program (2013R1A2A1A01015232) through the National Research Foundation (NRF), funded by the Ministry of Science, ICT, & Future Planning. We would like to thank Prof. Jong-Jin Park at Chungnam National University for the preparation of conductive composite elastomer.

Supporting Information Available: This material is available free of charge *via* the Internet at http://pubs.acs.org.

REFERENCES AND NOTES

1. Yamada, T.; Hayamizu, Y.; Yamamoto, Y.; Yomogida, Y.; Izadi-Najafabadi, A.; Futaba, D. N.; Hata, K. A Stretchable Carbon Nanotube Strain Sensor for Human-Motion Detection. *Nat. Nanotechnol.* **2011**, *6*, 296–301.
2. Najafi, B.; Aminian, K.; Paraschiv-Ionescu, A.; Loew, F.; Bula, C. J.; Robert, P. Ambulatory System for Human Motion Analysis Using a Kinematic Sensor: Monitoring of Daily Physical Activity in the Elderly. *IEEE Trans. Biomed. Eng.* **2003**, *50*, 711–723.
3. Lim, S.; *et al.* Transparent and Stretchable Interactive Human Machine Interface Based on Patterned Graphene Heterostructures. *Adv. Funct. Mater.* **2015**, *25*, 375–383.
4. Jung, S.; Kim, J. H.; Kim, J.; Choi, S.; Lee, J.; Park, I.; Hyeon, T.; Kim, D.-H. Reverse-Micelle-Induced Porous Pressure-Sensitive Rubber for Wearable Human–Machine Interfaces. *Adv. Mater.* **2014**, *26*, 4825–4830.
5. Kim, J. *et al.* Stretchable Silicon Nanoribbon Electronics for Skin Prosthesis. *Nat. Commun.* **2014**, *5*, 5747.
6. Tien, N. T.; Jeon, S.; Kim, D.-I.; Trung, T. Q.; Jang, M.; Hwang, B.-U.; Byun, K.-E.; Bae, J.; Lee, E.; Tok, J. B.-H.; *et al.* A Flexible

Bimodal Sensor Array for Simultaneous Sensing of Pressure and Temperature. *Adv. Mater.* **2014**, *26*, 796–804.
7. Trung, T. Q.; Ramasundaram, S.; Hong, S. W.; Lee, N.-E. Flexible and Transparent Nanocomposite of Reduced Graphene Oxide and P(VDF-TrFE) Copolymer for High Thermal Responsivity in a Field-Effect Transistor. *Adv. Funct. Mater.* **2014**, *24*, 3438–3445.
8. Kim, K. H.; Bang, S. W.; Kim, S. R. Emotion Recognition System Using Short-Term Monitoring of Physiological Signals. *Med. Biol. Eng. Comput.* **2004**, *42*, 419–427.
9. Sixsmith, A.; Johnson, N. A Smart Sensor to Detect the Falls of the Elderly. *IEEE Pervasive Comput.* **2004**, *3*, 42–47.
10. Aggarwal, J. K.; Ryoo, M. S. Human Activity Analysis: A Review. *ACM Comput. Surv.* **2011**, *43*, 1–43.
11. Trung, T. Q.; Tien, N. T.; Kim, D.; Jang, M.; Yoon, O. J.; Lee, N.-E. A Flexible Reduced Graphene Oxide Field-Effect Transistor for Ultrasensitive Strain Sensing. *Adv. Funct. Mater.* **2014**, *24*, 117–124.
12. Park, J. J.; Hyun, W. J.; Mun, S. C.; Park, Y. T.; Park, O. O. Highly Stretchable and Wearable Graphene Strain Sensors with Controllable Sensitivity for Human Motion Monitoring. *ACS Appl. Mater. Interfaces* **2015**, *7*, 6317–6324.
13. Calder, A. J.; Young, A. W. Understanding the Recognition of Facial Identity and Facial Expression. *Nat. Rev. Neurosci.* **2005**, *6*, 641–651.
14. Lee, J.; Kim, S.; Lee, J.; Yang, D.; Park, B. C.; Ryu, S.; Park, I. A Stretchable Strain Sensor Based on a Metal Nanoparticle Thin Film for Human Motion Detection. *Nanoscale* **2014**, *6*, 11932–11939.
15. Bae, S.-H.; Lee, Y.; Sharma, B. K.; Lee, H.-J.; Kim, J.-H.; Ahn, J.-H. Graphene-Based Transparent Strain Sensor. *Carbon* **2013**, *51*, 236–242.
16. Xiao, X.; Yuan, L.; Zhong, J.; Ding, T.; Liu, Y.; Cai, Z.; Rong, Y.; Han, H.; Zhou, J.; Wang, Z. L. High-Strain Sensors Based on ZnO Nanowire/Polystyrene Hybridized Flexible Films. *Adv. Mater.* **2011**, *23*, 5440–5444.
17. Yan, C.; Wang, J.; Kang, W.; Cui, M.; Wang, X.; Foo, C. Y.; Chee, K. J.; Lee, P. S. Highly Stretchable Piezoresistive Graphene–Nanocellulose Nanopaper for Strain Sensors. *Adv. Mater.* **2014**, *26*, 2022–2027.
18. Amjadi, M.; Pichitpajongkit, A.; Lee, S.; Ryu, S.; Park, I. Highly Stretchable and Sensitive Strain Sensor Based on Silver Nanowire–Elastomer Nanocomposite. *ACS Nano* **2014**, *8*, 5154–5163.
19. Boland, C. S.; Khan, U.; Backes, C.; O'Neill, A.; McCauley, J.; Duane, S.; Shanker, R.; Liu, Y.; Jurewicz, I.; Dalton, A. B.; Coleman, J. N. Sensitive, High-Strain, High-Rate Bodily Motion Sensors Based on Graphene–Rubber Composites. *ACS Nano* **2014**, *8*, 8819–8830.
20. Kong, J.-H.; Jang, N.-S.; Kim, S.-H.; Kim, J.-M. Simple and Rapid Micropatterning of Conductive Carbon Composites and its Application to Elastic Strain Sensors. *Carbon* **2014**, *77*, 199–207.
21. Cai, L.; Song, L.; Luan, P.; Zhang, Q.; Zhang, N.; Gao, Q.; Zhao, D.; Zhang, X.; Tu, M.; Yang, F.; *et al.* Super-Stretchable, Transparent Carbon Nanotube-Based Capacitive Strain Sensors for Human Motion Detection. *Sci. Rep.* **2013**, *3*.
22. Yao, S.; Zhu, Y. Wearable Multifunctional Sensors Using Printed Stretchable Conductors Made of Silver Nanowires. *Nanoscale* **2014**, *6*, 2345–2352.
23. Pang, C.; Lee, G.-Y.; Kim, T.-i.; Kim, S. M.; Kim, H. N.; Ahn, S.-H.; Suh, K.-Y. A Flexible and Highly Sensitive Strain-Gauge Sensor Using Reversible Interlocking of Nanofibres. *Nat. Mater.* **2012**, *11*, 795–801.
24. Lu, N.; Lu, C.; Yang, S.; Rogers, J. Highly Sensitive Skin-Mountable Strain Gauges Based Entirely on Elastomers. *Adv. Funct. Mater.* **2012**, *22*, 4044–4050.
25. Kang, D.; Pikhitsa, P. V.; Choi, Y. W.; Lee, C.; Shin, S. S.; Piao, L.; Park, B.; Suh, K.-Y.; Kim, T.-i.; Choi, M. Ultrasensitive Mechanical Crack-Based Sensor Inspired by the Spider Sensory System. *Nature* **2014**, *516*, 222–226.
26. Wang, Y.; Wang, L.; Yang, T.; Li, X.; Zang, X.; Zhu, M.; Wang, K.; Wu, D.; Zhu, H. Wearable and Highly Sensitive Graphene Strain Sensors for Human Motion Monitoring. *Adv. Funct. Mater.* **2014**, *24*, 4666–4670.
27. Slobodian, P.; Riha, P.; Benlikaya, R.; Svoboda, P.; Petras, D. A Flexible Multifunctional Sensor Based on Carbon Nanotube/Polyurethane Composite. *IEEE Sens. J.* **2013**, *13*, 4045–4048.
28. Kim, D.-H.; Lu, N.; Ma, R.; Kim, Y.-S.; Kim, R.-H.; Wang, S.; Wu, J.; Won, S. M.; Tao, H.; Islam, A.; *et al.* Epidermal Electronics. *Science* **2011**, *333*, 838–843.
29. Muth, J. T.; Vogt, D. M.; Truby, R. L.; Mengüç, Y.; Kolesky, D. B.; Wood, R. J.; Lewis, J. A. Embedded 3D Printing of Strain Sensors within Highly Stretchable Elastomers. *Adv. Mater.* **2014**, *26*, 6307–6312.
30. Kang, I.; Schulz, M. J.; Kim, J. H.; Shanov, V.; Shi, D. A Carbon Nanotube Strain Sensor for Structural Health Monitoring. *Smart Mater. Struct.* **2006**, *15*, 737–748.
31. Qiu, W.; Li, Q.; Lei, Z.-K.; Qin, Q.-H.; Deng, W.-L.; Kang, Y.-L. The Use of a Carbon Nanotube Sensor for Measuring Strain by Micro-Raman Spectroscopy. *Carbon* **2013**, *53*, 161–168.
32. Wang, Y.; Yang, R.; Shi, Z.; Zhang, L.; Shi, D.; Wang, E.; Zhang, G. Super-Elastic Graphene Ripples for Flexible Strain Sensors. *ACS Nano* **2011**, *5*, 3645–3650.
33. Tian, H.; Shu, Y.; Cui, Y.-L.; Mi, W.-T.; Yang, Y.; Xie, D.; Ren, T.-L. Scalable Fabrication of High-Performance and Flexible Graphene Strain Sensors. *Nanoscale* **2014**, *6*, 699–705.
34. Shin, M. K.; Oh, J.; Lima, M.; Kozlov, M. E.; Kim, S. J.; Baughman, R. H. Elastomeric Conductive Composites Based on Carbon Nanotube Forests. *Adv. Mater.* **2010**, *22*, 2663–2667.
35. Hu, N.; Karube, Y.; Arai, M.; Watanabe, T.; Yan, C.; Li, Y.; Liu, Y.; Fukunaga, H. Investigation on Sensitivity of a Polymer/Carbon Nanotube Composite Strain Sensor. *Carbon* **2010**, *48*, 680–687.
36. Mattmann, C.; Clemens, F.; Tröster, G. Sensor for Measuring Strain in Textile. *Sensors* **2008**, *8*, 3719–3732.
37. Toprakci, H. A. K.; Kalanadhabhatla, S. K.; Spontak, R. J.; Ghosh, T. K. Polymer Nanocomposites Containing Carbon Nanofibers as Soft Printable Sensors Exhibiting Strain-Reversible Piezoresistivity. *Adv. Funct. Mater.* **2013**, *23*, 5536–5542.
38. Lipomi, D. J.; Vosgueritchian, M.; Tee, B. C. K.; Hellstrom, S. L.; Lee, J. A.; Fox, C. H.; Bao, Z. Skin-Like Pressure and Strain Sensors Based on Transparent Elastic Films of Carbon Nanotubes. *Nat. Nanotechnol.* **2011**, *6*, 788–792.
39. Stutz, H.; Illers, K. H.; Mertes, J. A Generalized Theory for the Glass Transition Temperature of Crosslinked and Uncrosslinked Polymers. *J. Polym. Sci., Part B: Polym. Phys.* **1990**, *28*, 1483–1498.
40. Mustonen, T.; Kordás, K.; Saukko, S.; Tóth, G.; Penttilä, J. S.; Helistö, P.; Seppä, H.; Jantunen, H. Inkjet Printing of Transparent and Conductive Patterns of Single-Walled Carbon Nanotubes and PEDOT-PSS Composites. *Phys. Status Solidi* **2007**, *244*, 4336–4340.
41. Fragopanagos, N.; Taylor, J. G. Emotion Recognition in Human–Computer Interaction. *Neural Networks* **2005**, *18*, 389–405.
42. Cohen, I.; Sebe, N.; Garg, A.; Chen, L. S.; Huang, T. S. Facial Expression Recognition from Video Sequences: Temporal and Static Modeling. *Comput. Vision Image Understanding* **2003**, *91*, 160–187.
43. Samal, A.; Iyengar, P. A. Automatic Recognition and Analysis of Human Faces and Facial Expressions: A Survey. *Pattern Recognit.* **1992**, *25*, 65–77.
44. Pang, C.; Koo, J. H.; Nguyen, A.; Caves, J. M.; Kim, M.-G.; Chortos, A.; Kim, K.; Wang, P. J.; Tok, J. B.-H.; Bao, Z. Highly Skin-Conformal Microhairy Sensor for Pulse Signal Amplification. *Adv. Mater.* **2015**, *27*, 634–640.